AD-A182 140 AN EXPERIMENTAL INVESTIGATION OF THE AEROMECHANICAL STABILITY OF A HINGEL..(U) NATIONAL AERONAUTICS AND SPACE ADMINISTRATION HAMPTON VA LANG..

1/1

UNCLASSIFIED W T YEAGER ET AL. JUN 87 NASA-L-16280 F/G 20/4 NL

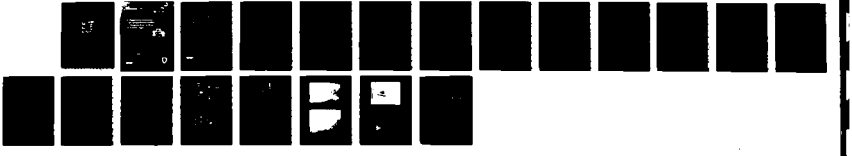

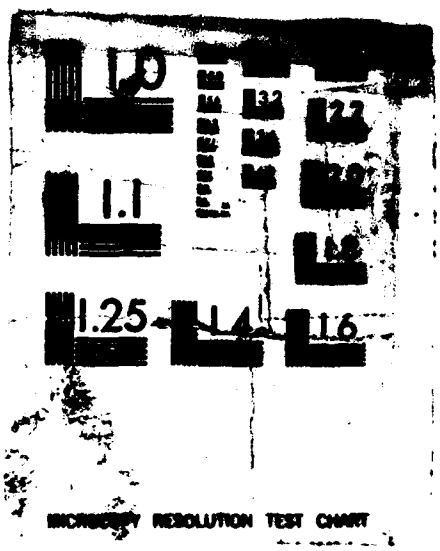
1.1
1.25
1.4
1.6
MICROCOPY RESOLUTION TEST CHART

[redacted]

[redacted]

[redacted]

[redacted]

NASA

NASA
Technical Memorandum 89107

AVSCOM
Technical Memorandum 87-B-5

An Experimental Investigation of the Aeromechanical Stability of a Hingeless Rotor in Hover and Forward Flight

William T. Yeager, Jr.
Aerostructures Directorate
USAARTA-AVSCOM
Langley Research Center
Hampton, Virginia

M-Nabil H. Hamouda
PRC Kentron, Inc.
Hampton, Virginia

Wayne R. Mantay
Aerostructures Directorate
USAARTA-AVSCOM
Langley Research Center
Hampton, Virginia

National Aeronautics and Space Administration

Scientific and Technical Information Office

1987

The use of trademarks or names of manufacturers in this report is for accurate reporting and does not constitute an official endorsement, either expressed or implied, of such products or manufacturers by the National Aeronautics and Space Administration.

Summary

Analysis and testing were conducted in the Langley Transonic Dynamics Tunnel to investigate the aeromechanical stability of a soft inplane hingeless rotor model. Rotor stability data were obtained in hover and in forward flight up to an advance ratio of 0.35. Model rotor parameters evaluated were blade sweep and droop, pre-cone of the blade feathering axis, and blade pitch-flap coupling. Data obtained during these tests are presented herein without analysis.

Introduction

The aeromechanical stability of a helicopter rotor system is an area which is of concern to the designer. Aeromechanical stability problems involve the interaction of the rotor and the airframe and are usually divided into the categories of ground resonance and air resonance. Although the terminology may imply totally different phenomena, both are self-excited instabilities caused by the coupling between blade lagging motion and hub motion in the plane of the rotor (refs. 1 to 3). Although aeromechanical instability is traditionally associated with articulated rotors, hingeless rotors are also susceptible to these problems. Hingeless rotors are classified into two types. One type is associated with a soft inplane system which has the blade inplane frequency less than the rotor rotational speed, and the second type is associated with a stiff inplane system which has the blade inplane frequency more than the rotor rotational speed. The information in this report deals with the aeromechanical stability of a soft inplane hingeless rotor system.

Aeromechanical stability is a well understood phenomenon (ref. 4), particularly for articulated rotors. However, hingeless rotors provide substantial structural and aerodynamic couplings that complicate their aeromechanical stability problems. Analytical models (refs. 5 to 8) have been developed to investigate the aeromechanical stability of hingeless rotors. Correlation efforts with these analyses (refs. 9 to 11) have generally been confined to hover and the use of small-scale models in forward flight.

Wind-tunnel tests have been conducted at the Langley Transonic Dynamics Tunnel (TDT) to investigate the aeromechanical stability of a soft inplane hingeless rotor system. These tests had several objectives: (1) development and evaluation of an experimental technique for blade excitation and damping measurements in the rotating system, (2) acquisition of a data base for hingeless rotor aeromechanical stability, and (3) evaluation of an analysis that can be used at the TDT during the design and testing phases of hingeless and bearingless rotor development. The analysis that was evaluated during these tests was the Comprehensive Analytical Model of Rotorcraft Aerodynamics and Dynamics (CAMRAD) described in reference 8. The TDT tests obtained rotor stability data in hover and in forward flight. The effects on rotor stability of rotor-hub geometric parameters were investigated. These parameters were blade sweep and droop, pre-cone of the blade feathering axis, and blade pitch-flap coupling. Comparisons between theory and selected experimental data from the TDT are presented in reference 12. All data from the TDT tests are presented without analysis.

Symbols

AMP	amplitude of transient response
b	number of blades
C_L	rotor lift coefficient, $L/\rho\pi R^2(\Omega R)^2$
c	blade chord, ft
FFT	fast Fourier transform
f	rotor lead-lag frequency, Hz
L	rotor lift, lb
$L(A)$	natural logarithm of amplitude of transient response
R	rotor radius, ft
RS	blade radial station, in.
r	spanwise distance along blade radius measured from center of rotation, ft
V	tunnel free-stream velocity, ft/sec
α_s	rotor shaft angle of attack (positive for rotor tilted rearward), deg
δ_3	blade pitch-flap coupling (positive for flap up, pitch down), deg
ζ	lead-lag damping ratio, percent critical
θ	blade collective pitch angle, deg
μ	rotor advance ratio, $V/\Omega R$
ρ	test-medium mass density, slug/ft^3
σ	rotor solidity, $bc/\pi R$
Ω	rotor rotational velocity, rpm

Apparatus and Procedures

Wind Tunnel

The tests were conducted in the Langley Transonic Dynamics Tunnel (TDT). A schematic of the

tunnel is shown in figure 1. This tunnel is a continuous-flow tunnel with a slotted test section. The tunnel test section is 16 ft square with cropped corners and has a cross-sectional area of 248 ft^2. Either air or Freon 12[1] may be used as a test medium. For this investigation, Freon 12 at a nominal density of 0.0047 $slug/ft^3$ was used as the test medium. Because of its high density and low speed of sound, the use of Freon 12 aids the matching of model-rotor-scale Reynolds number and Mach number to full-scale values. The heavier test medium permits a simplified structural design to obtain the required stiffness characteristics for dynamic similarity, and thus eases design and fabrication requirements of the model (ref. 13).

Model Description

The rotor model used for this investigation is a soft inplane hingeless rotor, the properties of which are listed in tables I and II. The rotor lead-lag and flap frequencies listed in table I were calculated from the analysis of reference 8 and are based on a nominal rotor speed of 618 rpm. A sketch of the model rotor hub and blade assembly is shown in figure 2. The model blades were fabricated with fiberglass spars specifically for testing in the Freon 12 test medium of the TDT.

The model rotor hub, shown in figure 3, consists of metal flexures to accommodate flap and lead-lag motions and a mechanical feathering bearing to allow blade pitch motion. The flap and lead-lag flexures contain strain gages calibrated to measure motion in those directions. The hingeless hub has the capability to independently vary blade sweep, droop, and pre-cone of the blade feathering axis. The changes are accomplished by means of angle blocks as shown in figure 4. Two values of blade pitch-flap coupling are obtained by the use of spacers placed between the pitch horn and the pitch link. A list of rotor configurations tested is given in table III.

The test bed used for this investigation was the aeroelastic rotor experimental system (ARES) model. The ARES model, shown in figure 5, consists of a rotor drive system and rotor control system enclosed by a streamlined helicopter fuselage shape. The ARES model utilizes a six-component strain-gage balance to measure rotor forces and moments. The balance is fixed with respect to the rotor shaft and thus pitches with the model. Fuselage forces and moments are not sensed by the balance. The entire ARES model and balance assembly are mounted on a rigid stand bolted to the floor of the wind tunnel. The measured frequency and damping values of the ARES model as mounted in the tunnel were determined from a "bump" test and are presented in table IV. The ARES model rotor control system and fuselage pitch attitude are remotely controlled from within the wind-tunnel control room. The swashplate is moved by three hydraulic actuators. Instrumentation on the ARES model and in the wind-tunnel control room allows continuous displays of model control settings, rotor forces and moments, blade loads, and pitch link loads. The ARES model pitch attitude is measured by an accelerometer, and rotor control positions are measured by linear potentiometers connected to the swashplate. Rotating system data are transferred into the fixed system through a 30-channel slipring assembly.

Test Procedures

During this investigation, data were taken at several rotor rpm values. At each test point the tunnel speed was adjusted to give the desired rotor advance ratio. The model was then pitched to a specified shaft angle of attack and the collective pitch was set. Cyclic pitch control was used to remove the rotor first harmonic flapping with respect to the shaft. Once the test condition was established, multiple measurements of rotor inplane frequency and damping in the rotating system were made with the moving-block method (ref. 14) used as an interactive program.

The test technique consisted of two steps. First, the model was excited in the fixed system by applying a longitudinal cyclic pitch oscillation to the rotor through the swashplate. The magnitude of the swashplate oscillation was nominally 0.75°. The frequency of the swashplate oscillation was initially set equal to the fixed-system value of the rotor inplane frequency (lead-lag regressing mode) predicted by CAMRAD as described in reference 12. The swashplate oscillation frequency was then adjusted slightly to obtain the maximum rotor inplane response. Once the rotor inplane response was established, the swashplate oscillation was removed and the moving-block procedure was initiated. A typical real-time moving-block display is shown in figure 6. This display was utilized as described in reference 14. The frequency of interest was selected from the fast Fourier transform (FFT) of the lead-lag signal trace, and the damping ratio was computed from the natural logarithm of the amplitude of the filtered lead-lag response. When a condition of negative damping was achieved, the swashplate excitation was removed and the rotor rotational speed was immediately reduced. This action was sufficient to eliminate the rotor disturbance in the unstable region.

[1] Freon registered trademark of E. I. du Pont de Nemours & Co., Inc.

Presentation of Results

The rotor stability data obtained during this investigation are presented as tabulated values of the rotor lead-lag frequency and damping in the rotating system. These data are presented for each test condition and model rotor configuration. The data were taken in hover and in forward flight up to an advance ratio of 0.35. Multiple measurements of rotor frequency and damping are presented at most test conditions. The data are presented in the following order:

Concluding Remarks

Aeromechanical stability data, in the form of lead-lag damping and frequency, have been obtained for a soft inplane hingeless rotor model. These data were obtained in hover and in forward flight for several model configurations. These data may be useful for validating existing rotor aeromechanical stability analyses used in the design of hingeless and bearingless rotor systems.

NASA Langley Research Center
Hampton, VA 23665-5225

March 30, 1987

References

1. Hohenemser, Kurt H.: *Hingeless Rotorcraft Flight Dynamics*. AGARD-AG-197, Sept. 1974.
2. Donham, R. E.; Cardinale, S. V.; and Sachs, I. B.: Ground and Air Resonance Characteristics of a Soft In-Plane Rigid-Rotor System. *J. American Helicopter Soc.*, vol. 14, no. 4, Oct. 1969, pp. 33–41.
3. Miao, Wen-Liu; and Huber, Helmut B.: Rotor Aeroelastic Stability Coupled With Helicopter Body Motion. *Rotorcraft Dynamics*, NASA SP-352, 1974, pp. 137–146.
4. Coleman, Robert P.; and Feingold, Arnold M. (appendix B by George W. Brooks): *Theory of Self-Excited Mechanical Oscillations of Helicopter Rotors With Hinged Blades*. NACA Rep. 1351, 1958. (Supersedes NACA TN 3844.)
5. Young, Maurice I.; and Bailey, David J.: Stability and Control of Hingeless Rotor Helicopter Ground Resonance. *J. Aircr.*, vol. 11, no. 6, June 1974, pp. 333–339.
6. Ormiston, Robert A.: Aeromechanical Stability of Soft Inplane Hingeless Rotor Helicopters. *Third European Rotorcraft and Powered Lift Aircraft Forum*, Association Aeronautique et Astronautique de France, Sept. 1977, Paper No. 25.
7. Hodges, Dewey H.: A Theoretical Technique for Analysing Aeroelastic Stability of Bearingless Rotors. *A Collection of Technical Papers—AIAA/ASME 19th Structures, Structural Dynamics and Materials Conference*, c.1978, pp. 282–294.
8. Johnson, Wayne: *A Comprehensive Analytical Model of Rotorcraft Aerodynamics and Dynamics. Part 1: Analysis Development*. NASA TM-81182, AVRADCOM TR-80-A-5, 1980.
9. Burkam, John E.; and Miao, Wen-Liu: Exploration of Aeroelastic Stability Boundaries With a Soft-in-Plane Hingeless-Rotor Model. *J. American Helicopter Soc.*, vol. 17, no. 4, Oct. 1972, pp. 27–35.
10. Bousman, William G.: *An Experimental Investigation of Hingeless Helicopter Rotor-Body Stability in Hover*. NASA TM-78489, AVRADCOM TR 78-17(AM), 1978.
11. Weller, William H.: *Correlating Measured and Predicted Inplane Stability Characteristics for an Advanced Bearingless Rotor*. NASA CR-166280, 1982.
12. Yeager, William T., Jr.; Hamouda, M-Nabil H.; and Mantay, Wayne R.: *Aeromechanical Stability of a Hingeless Rotor in Hover and Forward Flight: Analysis and Wind Tunnel Tests*. NASA TM-85683, AVRADCOM TR 83-B-5, 1983.
13. Lee, Charles: Weight Considerations in Dynamically Similar Model Rotor Design. SAWE Paper No. 659, May 1968.
14. Hammond, Charles E.; and Doggett, Robert V., Jr.: Determination of Subcritical Damping by Moving-Block/Randomdec Applications. *Flutter Testing Techniques*, NASA SP-415, 1976, pp. 59–76.

Table I. Principal Rotor Model Properties

Number of blades	4
Rotor diameter, ft	9
Blade chord, ft	0.353
Solidity	0.10
Airfoil section	NACA 0012
Blade twist, deg	0
Blade elastic axis, percent chord	25
Blade pitch axis, percent chord	25
Blade center of gravity, percent chord	25
Flap flexure weight, lb	0.55
Pitch-bearing-housing weight, lb	1.13
Lead-lag flexure weight, lb	0.80
Flap flexure stiffness in flap direction, lb-in^2	3984.0
Lead-lag flexure stiffness in lead-lag direction, lb-in^2	12165.0
Lead-lag flexure torsional stiffness, lb-in^2	11080
Control system stiffness, in-lb/rad	2331
First flap frequency (calculated),[a] per revolution	1.14
First lead-lag frequency (calculated),[a] per revolution	0.55

[a]$\Omega = 618$ rpm.

Table II. Rotor Model Blade Structural Properties

[Assumed modulus of elasticity for blade is 10^6 lb/in^2]

Inboard station, r/R	Segment length, in.	Weight, lb/in.	Torsional inertia, lb-sec^2	Torsional stiffness, lb-in^2	Edgewise area moment of inertia, in^4	Flatwise area moment of inertia, in^4
0.213	2.87	0.140	0.000144	43800.0	0.0268	0.00387
.266	.22	.031	.000072	34000.0	.0252	.00249
.269	2.25	.044	.000077	34000.0	.0252	.00249
.311	5.90	.041	.000075	23500.0	.0304	.00231
.420	4.50	.040	.000073	19700.0	.0264	.00181
.503	22.75	.039	.000071	16900.0	.0245	.00151
.924	1.75	.039	.000071	16900.0	.0245	.00151
.957	.25	.041	.000073	17500.0	.0245	.00160
.961	1.00	.079	.000103	50000.0	.0500	.00500
.980	.25	.061	.000092	40000.0	.0400	.00405
.984	.75	.011	.000011	50000.0	.0050	.00050

Table III. Rotor Configuration Parametric Values

Configuration	δ_3, deg	Sweep,[a] deg	Droop,[b] deg	Pre-cone,[c] deg
Baseline	0	0	0	0
1	26	0	0	0
2	0	0	2	0
3	0	2	0	0
4	26	0	2	3
5	26	0	−2	3
6	26	0	4	3
7	26	0	4	6

[a]Positive aft.
[b]Positive down.
[c]Positive up.

Table IV. Measured ARES Model Dynamic Properties

Mode	Frequency,[a] Hz	Damping,[a] percent critical
Roll	5.4	7.3
Pitch	5.9	5.7

[a]Includes simulated rotor mass.

Table V. Lead-Lag Frequency and Damping for Baseline Configuration in Hover at $\alpha_s = 0°$

	Frequency and damping for θ, deg, of—									
	0		4		8		[a]11		13	
Ω, rpm	f, Hz	ζ, percent critical	f, Hz	ζ, percent critical	f, Hz	ζ, percent critical	f, Hz	ζ, percent critical	f, Hz	ζ, percent critical
400	4.87	0.37	4.80	0.45	4.90	0.53	4.94	2.08	4.94	1.06
	4.90	.35	4.83	.42	4.90	.89	4.98	1.98		
	4.87	.38	4.87	.67	4.90	1.30	4.90	2.42		
			4.87	.67	4.90	1.06	4.90	1.77		
450	5.13	0.46	5.13	0.61	5.05	0.71	5.17	2.81	5.25	2.36
	5.09	.48	5.13	.72	5.17	1.11	5.21	2.27		
	5.13	.63	5.09	.57	5.13	1.06	5.21	1.86		
					5.13	1.09				
500	5.42	0.57	5.44	0.69	5.38	0.49	5.51	1.81	5.51	3.12
	5.42	.67	5.42	.69	5.42	1.28	5.46	2.10	5.46	3.21
	5.38	.68	5.38	.70	5.42	1.22	5.46	1.95		
					5.42	1.26				
550	5.68	0.55	5.68	0.55	5.65	0.44	5.72	2.26	5.76	2.89
	5.68	.56	5.68	.55	5.56	.56	5.76	2.07		
	5.68	.52	5.68	.66	5.65	.40	5.76	2.44		
					5.72	1.19				
					5.72	1.25				
					5.72	1.10				
600	5.98	0.55	5.98	0.49	5.85	0.42	6.03	2.16	5.89	3.14
	5.94	.62	5.98	.51	5.98	1.12	6.03	1.86	6.03	2.83
	5.94	.59	5.98	.47	5.98	1.12	6.03	2.49	5.94	3.01
					5.98	1.21				
618	6.03	0.53	6.08	−0.08	5.95	0.40	6.08	0.56	6.08	1.97
	6.03	.46			6.03	−.03	6.08	.46	6.08	1.87
	6.03	.52			6.08	1.19	6.08	.53	6.08	1.32
					6.12	−.05				
					6.08	.05				
630	6.12	0.35	6.08	0.26	6.17	−0.11	6.22	0.31	6.22	0.82
	6.08	.46	6.12	−.44	6.22	−.02	6.22	.31	6.22	.75
	6.12	.38	6.17	−.52	6.17	−.10	6.22	.30	6.17	.90
640	6.17	0.41								
	6.17	.42								
	6.17	.34								
650	6.32	−0.06	6.32	−0.31	6.32	−0.12	6.38	0.44	6.38	0.55
	5.98	−.48	6.38	−.29			6.38	.39	6.43	.88
	6.32	−.33	6.32	−.17			6.32	.13	6.38	.94

[a]Nominal θ to achieve "1g" condition of $C_L/\sigma = 0.07$.

Table VI. Lead-Lag Frequency and Damping for Configuration 1 in Hover at $\alpha_s = 0°$ and $\theta = 8°$

Ω, rpm	f, Hz	ζ, percent critical
400	4.94	1.26
450	5.17	1.95
500	5.51	1.16
550	5.72	1.73
600	5.98	1.35
618	6.08	1.26
630	6.17	1.25
640	6.17	−.38
650	6.27	−.51

Table VII. Lead-Lag Frequency and Damping for Baseline Configuration in Forward Flight

(a) $\mu = 0.15$; $\alpha_s = -1.3°$

Ω, rpm	Frequency and damping for θ, deg, of—			
	0		4	
	f, Hz	ζ, percent critical	f, Hz	ζ, percent critical
550	5.68	0.82	5.68	1.19
	5.64	.76	5.68	1.17
	5.68	.69	5.68	1.18
600	5.94	0.52	5.94	0.35
	5.94	.43	5.98	.38
	5.94	.43	5.94	.50
618	6.08	−0.58	6.03	−0.59
	6.03	−.43	6.03	−.56
	6.03	−.04	6.03	−.56

(b) $\mu = 0.20$; $\alpha_s = -2.3°$

Ω, rpm	Frequency and damping for θ, deg, of—			
	0		4	
	f, Hz	ζ, percent critical	f, Hz	ζ, percent critical
550	5.68	0.65	5.68	1.23
	5.68	.70	5.72	1.22
	5.68	.61	5.68	1.23
600	5.94	0.52	5.94	0.32
	5.94	.50	5.94	.41
	5.94	.42	5.94	.30
618	6.03	−0.19	6.08	−0.47
	6.03	−.08	6.08	−.63
	6.03	−.12	6.03	−.63

Table VII. Concluded

(c) $\mu = 0.30$; $\alpha_s = -5.2°$

Ω, rpm	Frequency and damping for θ, deg, of—			
	0		4	
	f, Hz	ς, percent critical	f, Hz	ς, percent critical
550	5.72	0.73	5.72	1.09
	5.72	.75	5.68	1.12
	5.72	.70	5.68	1.02
600	5.94	0.30	5.94	0.34
	5.98	.21	5.94	.09
	5.98	.16	5.94	.36
618	6.08	−0.57	6.12	−0.59
	6.08	−.62	5.98	−.38
	6.08	−.56	6.03	−.59

(d) $\mu = 0.35$; $\alpha_s = -7.1°$

Ω, rpm	Frequency and damping for θ, deg, of—			
	0		4	
	f, Hz	ς, percent critical	f, Hz	ς, percent critical
550	5.68	0.45	5.72	0.89
	5.68	.60	5.72	.81
	5.72	.48	5.72	.76
600	5.98	0.09	5.94	0.01
	5.98	.05	5.94	.21
	5.98	−.03	5.98	.00
618	6.08	−0.68	6.12	−0.48
	6.12	−.73	6.03	−.64
	6.07	−.69	6.12	−.65

Table VIII. Lead-Lag Frequency and Damping for Baseline Configuration in Forward Flight at $\Omega = 618$ rpm

θ, deg	α_s, deg	μ	f, Hz	ς
2	0	0.20	5.94	0.23
		.30		
4	0	0.20	5.98	0.28
			5.98	.68
			5.95	.08
			5.94	.49
			5.94	.33
			5.94	.55
		.30	5.98	.33
			5.94	.77
8	−5	0.20	6.08	1.93
		.30	6.03	1.71
			6.03	2.12
12	−10	0.20		
		.30	6.08	2.41

Table IX. Lead-Lag Frequency and Damping for Configuration 1 in Forward Flight at $\Omega = 618$ rpm

θ, deg	α_s, deg	μ	f, Hz	ς
4	0	0.20	6.17	0.58
			6.12	.70
		.30	6.08	.92
8	−5	0.20	6.12	2.20
			6.08	1.57
		.30	6.08	1.29
			6.08	1.27
12	−10	0.20	6.12	2.02
		.30	6.17	1.81

Table X. Lead-Lag Frequency and Damping for Configuration 2 in Forward Flight at $\Omega = 618$ rpm $[\mu = 0.20]$

θ, deg	α_s, deg	f, Hz	ς
4	0	6.03	0.60
8	−5	6.08	1.40
12	−10	6.22	2.29
		6.08	2.20

Table XI. Lead-Lag Frequency and Damping for Configuration 3 in Forward Flight at $\Omega = 618$ rpm

θ, deg	α_s, deg	μ	f, Hz	ς
4	0	0.20	6.08	1.00
		.30	6.08	1.10
8	−5	0.20	6.08	1.69
		.30	6.08	1.65
12	−10	0.20	6.12	2.95
			6.17	2.67
		.30	6.08	2.82

Table XII. Lead-Lag Frequency and Damping for Configuration 4 in Forward Flight at $\Omega = 618$ rpm

θ, deg	α_s, deg	μ	f, Hz	ς
4	0	0.20		
		.30	6.08	0.70
8	−5	0.20	6.08	1.39
		.30	6.12	1.32
12	−10	0.20	6.12	2.08
		.30	6.17	1.90

Table XIII. Lead-Lag Frequency and Damping for Configuration 5 in Forward Flight at $\Omega = 618$ rpm

θ, deg	α_s, deg	μ	f, Hz	ζ
4	0	0.20	6.08	1.37
			6.08	1.62
		.30	6.03	1.50
8	−5	0.20	5.98	2.50
		.30	5.98	2.47
12	−10	0.20	6.03	3.21
		.30	5.94	3.28

Table XIV. Lead-Lag Frequency and Damping for Configuration 6 in Forward Flight at $\Omega = 618$ rpm

θ, deg	α_s, deg	μ	f, Hz	ζ
4	0	0.20	6.08	0.60
		.30	6.03	.76
8	−5	0.20	6.08	0.80
		.30	6.12	.79
12	−10	0.20	6.12	1.61
		.30	6.12	1.80

Table XV. Lead-Lag Frequency and Damping for Configuration 7 in Forward Flight at $\Omega = 618$ rpm

θ, deg	α_s, deg	μ	f, Hz	ζ
4	0	0.20	6.12	1.30
		.30	5.98	1.29
			6.03	1.03
8	−5	0.20	6.12	1.42
		.30	6.17	1.24
			6.08	1.68
12	−10	0.20	6.22	2.66
		.30	6.12	2.58

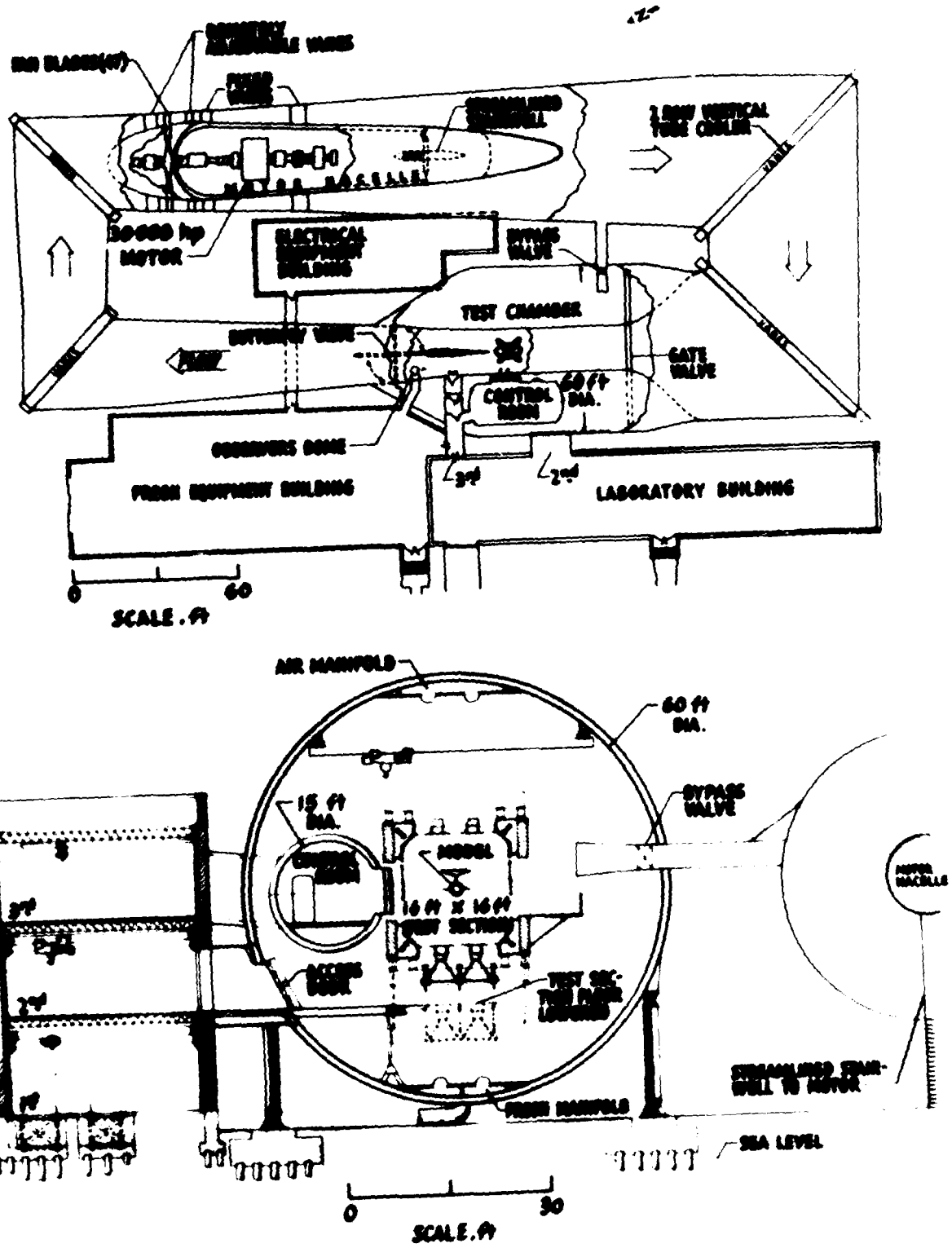

Figure 1 Langley Transonic Dynamics Tunnel

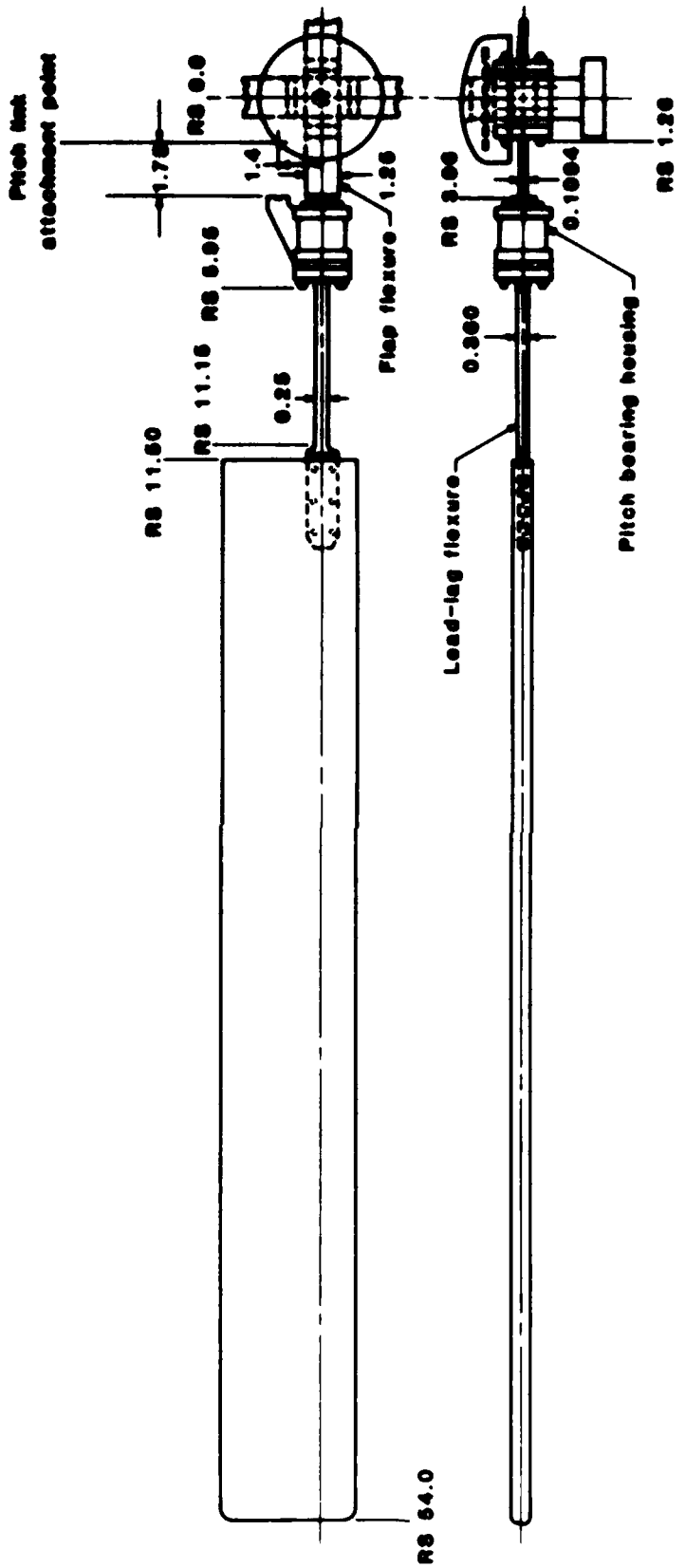

Figure 2. Model rotor hub and blade assembly. All dimensions are in inches.

L-83-5292

Figure 3. Model rotor hub.

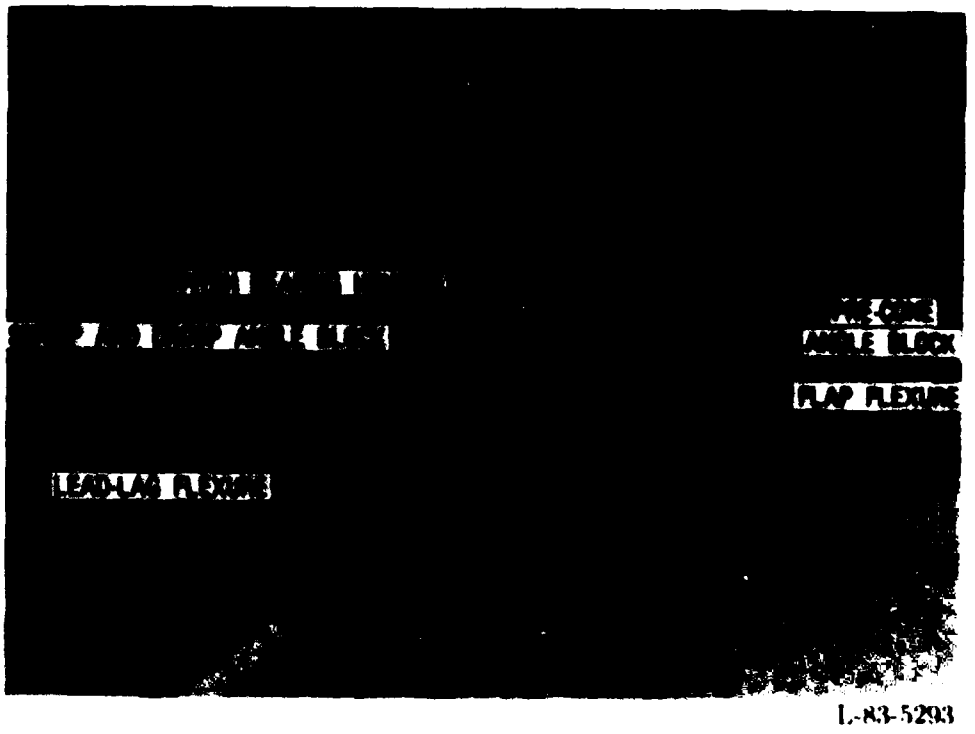

L-83-5293

Figure 4. Details of rotor-hub root flexures.

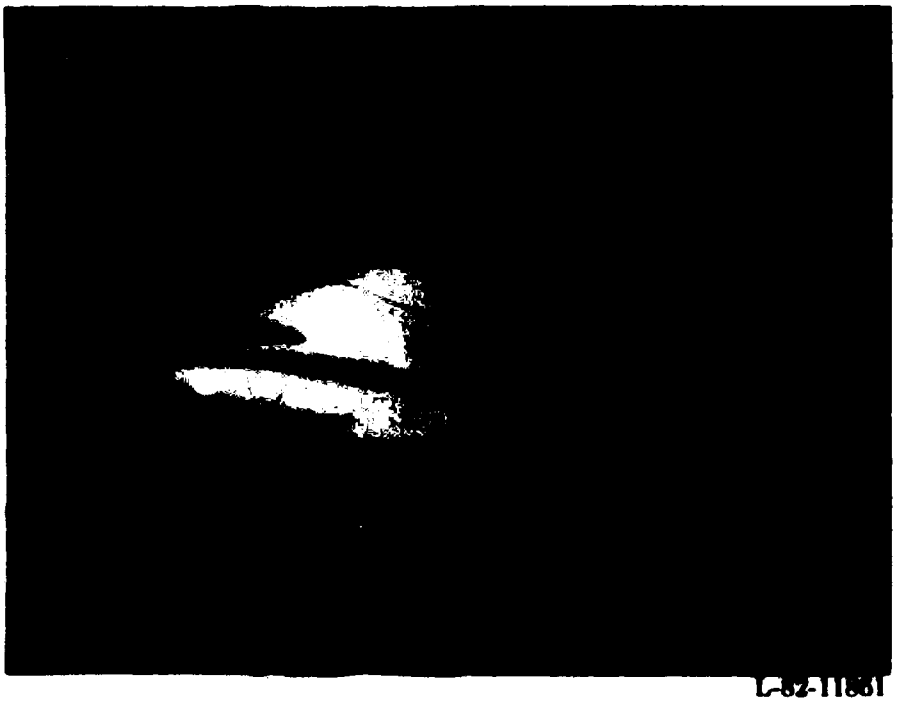

Figure 5. ARES mounted in Langley Transonic Dynamics Tunnel.

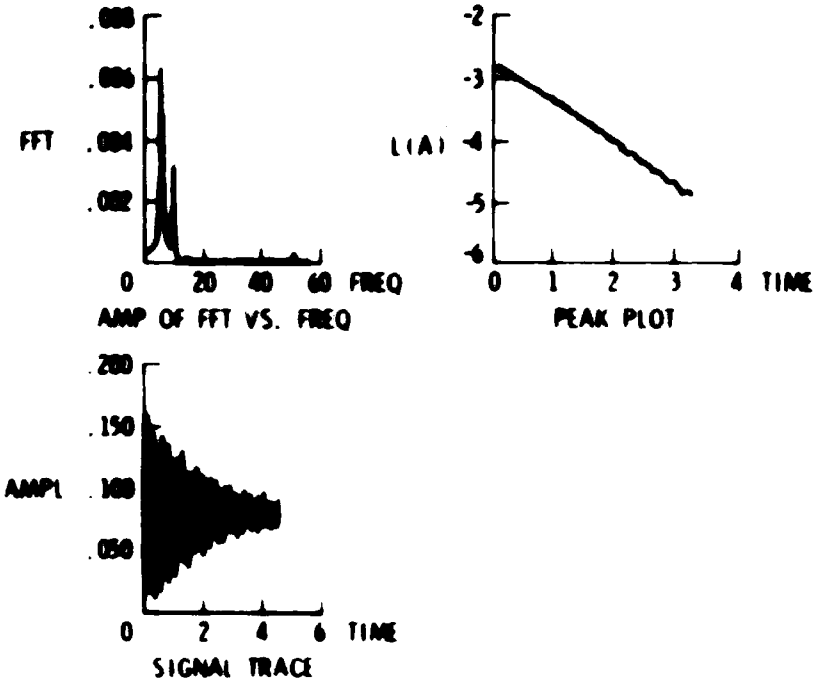

Figure 6. Sample real-time display of moving block results.

END

7-87

DTIC